Electronic Supplementary Information of

Multi-beam single-molecule defocused fluorescence imaging reveals local anisotropic nature of polymer thin films

Satoshi Habuchi, Tatsuya Oba, Martin Vacha**

Department of Organic and Polymeric Materials, Tokyo Institute of Technology, Ookayama, Meguro-ku, Tokyo 152-8552, Japan

Tel.: +81-3-5734-3643, Fax: +81-3-5734-2425, E-mail: habuchi.s.aa@m.titech.ac.jp, vacha.m.aa@m.titech.ac.jp

Calculation of excitation efficiency

Transition probability (absorption rate, Γ) of a molecule in a sample plane is described by an equation,

$$\Gamma \propto (\boldsymbol{E} \cdot \boldsymbol{\mu}) \tag{1}$$

where $\boldsymbol{E}$ and $\boldsymbol{\mu}$ represent electric field vector at the sample and absorption transition dipole described by θ and ϕ, respectively. $\boldsymbol{E}$ and $\boldsymbol{\mu}$ are described by equations,

$$\boldsymbol{\mu} = \begin{pmatrix} \sin\theta\cos\phi \\ \sin\theta\sin\phi \\ \cos\theta \end{pmatrix} |\boldsymbol{\mu}| \tag{2}$$

$$\boldsymbol{E}_{epi} = \begin{pmatrix} \cos\psi_{epi} \\ \sin\psi_{epi} \\ 0 \end{pmatrix} |\boldsymbol{E}_{epi}| \tag{3}$$

$$\boldsymbol{E}_{tilt,left} = J\boldsymbol{E}_{epi} = \begin{pmatrix} \cos\eta\cos\psi_{tilt} \\ \sin\psi_{tilt} \\ \sin\eta\cos\psi_{tilt} \end{pmatrix} |\boldsymbol{E}_{tilt,left}| \tag{4}$$

$$\boldsymbol{E}_{tilt,right} = -J\boldsymbol{E}_{epi} = \begin{pmatrix} -\cos\eta\cos\psi_{tilt} \\ \sin\psi_{tilt} \\ \sin\eta\cos\psi_{tilt} \end{pmatrix} |\boldsymbol{E}_{tilt,right}| \tag{5}$$

where $\boldsymbol{E}_{epi}$, $\boldsymbol{E}_{tilt,left}$, and $\boldsymbol{E}_{tilt,right}$ represent electric field vectors for epi- and tilt

angle-illumination light (see also Figure 1a in the main text). J is a rotation matrix. Note that $|-sin\eta cos\psi_{tilt}| = sin\eta cos\psi_{tilt}$ in equation 4 and 5. Γ for epi- (Γ_{epi}) and tilt angle-illumination (Γ_{tilt}) can, therefore, be described by equations,

$$\Gamma_{epi} = \left(\boldsymbol{\mu} \cdot \boldsymbol{E}_{epi}\right)^2 = \begin{pmatrix} \sin\theta\cos\phi\cos\psi_{epi} \\ \sin\theta\sin\phi\sin\psi_{epi} \\ 0 \end{pmatrix}^2 \left(|\boldsymbol{\mu}||\boldsymbol{E}_{epi}|\right)^2 \quad (6)$$

$$= \left(\sin\theta\cos\phi\cos\psi_{epi} + \sin\theta\sin\phi\sin\psi_{epi}\right)^2 \left(|\boldsymbol{\mu}||\boldsymbol{E}_{epi}|\right)^2 \quad (7)$$

$$\Gamma_{tilt,left} = \left(\boldsymbol{\mu} \cdot \boldsymbol{E}_{tilt,left}\right)^2 = \left(\boldsymbol{\mu} \cdot \boldsymbol{E}^p_{tilt,left} + \boldsymbol{\mu} \cdot \boldsymbol{E}^s_{tilt,left}\right)^2 \quad (8)$$

$$= [(\sin\theta\cos\phi\cos\eta\cos\psi_{tilt}, 0, \cos\theta\sin\eta\cos\psi_{tilt}) + (0, \sin\theta\sin\phi\sin\psi_{tilt}, 0)]^2 \left(|\boldsymbol{\mu}||\boldsymbol{E}_{epi}|\right)^2 \quad (9)$$

$$= \left(|\sin\theta\cos\phi\cos\eta\cos\psi_{tilt} + \cos\theta\sin\eta\cos\psi_{tilt}| + |\sin\theta\sin\phi\sin\psi_{tilt}|\right)^2 \left(|\boldsymbol{\mu}||\boldsymbol{E}_{epi}|\right)^2 \quad (10)$$

$$\Gamma_{tilt,right} = \left(\boldsymbol{\mu} \cdot \boldsymbol{E}_{tilt,right}\right)^2 = \left(\boldsymbol{\mu} \cdot \boldsymbol{E}^p_{tilt,RIGHT} + \boldsymbol{\mu} \cdot \boldsymbol{E}^s_{tilt,RIGHT}\right)^2 \quad (11)$$

$$= [(\sin\theta\cos\phi(-\cos\eta)\cos\psi_{tilt}, 0, \cos\theta\sin\eta\cos\psi_{tilt}) + (0, \sin\theta\sin\phi\sin\psi_{tilt}, 0)]^2 \left(|\boldsymbol{\mu}||\boldsymbol{E}_{epi}|\right)^2 \quad (12)$$

$$= \left(|\sin\theta\cos\phi(-\cos\eta)\cos\psi_{tilt} + \cos\theta\sin\eta\cos\psi_{tilt}| + |\sin\theta\sin\phi\sin\psi_{tilt}|\right)^2 \left(|\boldsymbol{\mu}||\boldsymbol{E}_{epi}|\right)^2 \quad (13)$$

Therefore, Γ for multi beam-illumination (Γ_{multi}) can, therefore, be described by equation 14.

$$\Gamma_{multi} = \Gamma_{epi} + \Gamma_{tilt,left} + \Gamma_{tilt,right} \quad (14)$$

The data in Figure 1b and 1c were calculated by the equation 7 and 14, respectively. For numerical

calculations of Γ_{multi}, we used following parameters; $\psi_{epi} = 90°$, $\eta = 40°$, and $\psi_{tilt} = 0°$. We calculated Γ_{epi} for a circularly polarized light illumination condition ($\psi_{epi} = 0 - 360°$).

Calculation of the collection efficiency of emission

A spatial pattern of radiation of the dipole in a homogeneous medium ($P_\infty(\alpha, \phi)$) is described by,[1]

$$P_\infty^{(p)}(\alpha, \phi) = \frac{3}{8\pi}[\cos\theta \sin\alpha + \sin\theta \cos\phi \cos\alpha]^2 \quad (15)$$

$$P_\infty^{(s)}(\alpha, \phi) = \frac{3}{8\pi}\sin^2\theta \sin^2\phi \quad (16)$$

$$P_\infty(\alpha, \phi) = P_\infty^{(p)}(\alpha, \phi) + P_\infty^{(s)}(\alpha, \phi) \quad (17)$$

where $P_\infty^{(p)}(\alpha, \phi)$ and $P_\infty^{(s)}(\alpha, \phi)$ represent radiation patterns of *p*- and *s*-polarized light (see also Figure S1). The radiation patterns at $\theta = 0$, and 90° are depicted in Figure S2. The collection efficiency of the emission when the molecule has the orientation of emission transition dipole described by θ ($P_\infty(\theta)$) was calculated by equation,

$$P_\infty(\theta) = \int_{180-\alpha_{N.A.}}^{180+\alpha_{N.A.}} P_\infty(\alpha, \phi)\mathrm{d}\alpha\mathrm{d}\phi \quad (18)$$

$$\alpha_{N.A.} = \mathrm{asin}\left(\frac{\mathrm{N.A.}}{n_1}\right) \quad (19)$$

where N.A. represents numerical aperture of the microscope objective (N.A. = 1.3 for our experiments).

A spatial pattern of radiation of the dipole at a plane dielectric interface ($P(\alpha, \phi)$) is calculated by the following equations. n_1 and n_2 are refractive indices of the polymer and air ($n_1 = 1.5$ and $n_2 = 1.0$), respectively in our calculations. $n = n_2/n_1 = 0.667$. The radiation patterns were calculated separately for three different angle ranges.[1]

(a) $0° \le \alpha \le 90°, 0° \le \alpha_2 \le 90°$ ($\alpha = \alpha_2$, $\alpha_1 = arcsin(n \times sin\alpha_2)$)

$$P^{(p)}(\alpha_2, \phi) = \frac{3}{2\pi}\frac{n^3\cos^2\alpha_2(\cos\theta\sin\alpha_1 + \sin\theta\cos\phi\cos\alpha_1)^2}{(n\cos\alpha_1 + \cos\alpha_2)^2} \quad (20)$$

$$P^{(s)}(\alpha_2, \phi) = \frac{3}{2\pi}\frac{n^3\cos^2\alpha_2\sin^2\theta\sin^2\phi}{(\cos\alpha_1 + n\cos\alpha_2)^2} \quad (21)$$

(b) $90° \le \alpha \le 180° - \alpha_{1,c}$, $\alpha_{1,c} \le \alpha_1 \le 90°$ ($\alpha_1 = 180 - \alpha$, $\alpha_{1,c} = arcsin(n)$)

$$P^{(p)}(\alpha_1, \phi) = [\cos^2\theta \sin^2\alpha_1 + n^{-4}\sin^2\theta \cos^2\phi\,(\sin^2\alpha_1 - n^2)]g^{(p)}(\alpha_1) \quad (22)$$

$$g^{(p)}(\alpha_1) = n^2[(1+n^{-2})\sin^2\alpha_1 - 1]^{-1}g^{(s)}(\alpha_1) \quad (23)$$

$$g^{(s)}(\alpha_1) = \frac{3}{2\pi}(1-n^2)^{-1}\cos^2\alpha_1 \quad (24)$$

$$P^{(s)}(\alpha_1, \phi) = \sin^2\theta \sin^2\phi\, g^{(s)}(\alpha_1) \quad (25)$$

(c) $180° - \alpha_{1,c} \le \alpha \le 180°$, $0 \le \alpha_1 \le \alpha_{1,c}$ ($\alpha_1 = 180 - \alpha$, $\alpha_{1,c} = arcsin(n)$, $\alpha_2 = arcsin(sin(\alpha_1)/n)$)

$$P^{(p)}(\alpha_1, \phi) = \frac{3}{2\pi}\frac{\cos^2\alpha_1(n\cos\theta\sin\alpha_1 - \sin\theta\cos\phi\cos\alpha_2)^2}{(n\cos\alpha_1 + \cos\alpha_2)^2} \quad (26)$$

$$P^{(s)}(\alpha_1, \phi) = \frac{3}{2\pi}\frac{\cos^2\alpha_1\sin^2\theta\sin^2\phi}{(\cos\alpha_1 + n\cos\alpha_2)^2} \quad (27)$$

where $P^{(p)}(\alpha, \phi)$ and $P^{(s)}(\alpha, \phi)$ represent radiation patterns of *p*- and *s*-polarized light (see also Figure S1). The total radiation patterns were calculated by,

$$P(\alpha, \phi) = P^{(p)}(\alpha, \phi) + P^{(s)}(\alpha, \phi) \quad (28)$$

The radiation patterns at $\theta = 0$, and 90° are depicted in Figure S2.

The collection efficiency of the emission when the molecule has the orientation of emission transition dipole described by θ ($P(\theta)$) was calculated by equation,

$$P(\theta) = \int_{180-\alpha_{N.A.}}^{180+\alpha_{N.A.}} P\,(\alpha, \phi)\mathrm{d}\alpha\mathrm{d}\phi \quad (29)$$

$$\alpha_{N.A.} = \mathrm{asin}\left(\frac{\mathrm{N.A.}}{n_1}\right) \quad (30)$$

where N.A. represents numerical aperture of the microscope objective (N.A. = 1.3 for our experiments). Calculated $P_\infty(\theta)$ and $P(\theta)$ are displayed in Figure S3. As seen in Figuer S3, emission from in-plane oriented molecules is collected more efficiently than those from out-of-plane

oriented molecule in homogeneous medium by the factor of 2.5. Similar trend is observed for the molecule located at the polymer-air interface. In this case, emission from in-plane oriented molecules is collected roughly 3.5 time more efficient than those from out-of-plane molecules.

Orientation dependent fluorescence quantum yield at the polymer-air interface

Total powers radiated by electric dipoles lying on a dielectric interface ($L(z_0)$) can be connected to radiative rate constants ($k_r(z_0)$) by the equation,[2, 3]

$$\frac{k_r(z_0)}{k_r(\infty)} = \frac{L(z_0)}{L(\infty)} = \left[\frac{L(z_0)}{L(\infty)}\right]_{\parallel} \sin^2\theta + \left[\frac{L(z_0)}{L(\infty)}\right]_{\perp} \cos^2\theta \quad (31)$$

where $L(\infty)$ and $k_r(\infty)$ represent the total radiation power and radiative rate constant when the dipole is in the infinite medium. The suffixes $\parallel$ and $\perp$ denote the dipoles oriented parallel and perpendicular to the interface, respectively. The rate constant of excited-state deactivation in the infinite medium ($k_{fl}(\infty)$) and at the interface ($k_{fl}(z_0)$) are expressed as,

$$k_{fl}(\infty) = k_r(\infty) + k_{nr} = k_r(\infty)/\Phi_{fl}(\infty) \quad (32)$$

$$k_{fl}(z_0) = k_r(z_0) + k_{nr} = k_r(z_0)/\Phi_{fl}(z_0) \quad (33)$$

where k_{nr} is non-radiative rate constant. $\Phi_{fl}(\infty)$ and $\Phi_{fl}(z_0)$ are fluorescence quantum yield in the infinite medium and at the interface, respectively. Therefore, $k_{fl}(z_0)$ and $\Phi_{fl}(z_0)$ can be described as,

$$k_{fl}(z_0) = k_{nr} + \left\{\left[\frac{L(z_0)}{L(\infty)}\right]_{\parallel} \sin^2\theta + \left[\frac{L(z_0)}{L(\infty)}\right]_{\perp} \cos^2\theta\right\} k_r(\infty) \quad (34)$$

$$\Phi_{fl}(z_0) = \left\{\left[\frac{L(z_0)}{L(\infty)}\right]_{\parallel} \sin^2\theta + \left[\frac{L(z_0)}{L(\infty)}\right]_{\perp} \cos^2\theta\right\} k_r(\infty) \Big/ \left[k_{nr} + \left\{\left[\frac{L(z_0)}{L(\infty)}\right]_{\parallel} \sin^2\theta + \left[\frac{L(z_0)}{L(\infty)}\right]_{\perp} \cos^2\theta\right\} k_r(\infty)\right] \quad (35)$$

$[L(z_0)/L(\infty)]_{\parallel}$ and $[L(z_0)/L(\infty)]_{\perp}$ can be described as,

$$\left[\frac{L(z_0)}{L(\infty)}\right]_{\parallel} \sim l_{e,\parallel}^{(0)} = \frac{3l_{m,\perp}^{(0)} - l_{m,\parallel}^{(0)}}{n^2+1} \quad (36)$$

$$\left[\frac{L(z_0)}{L(\infty)}\right]_{\perp} \sim l_{e,\perp}^{(0)} = \frac{2n^2}{n^2+1} l_{m,\parallel}^{(0)} - \frac{n^2-5}{n^2+1} l_{m,\perp}^{(0)} - 2 \quad (37)$$

$$l_{m,\parallel}^{(0)} = \frac{1}{5}\frac{n^5-1}{n^2-1} - \frac{1}{2}\frac{n^2}{n+1}\left(1 - \frac{3n}{n^2+1}\right) - \frac{n^4 \ln\{(\sqrt{n^2+1}-n)(\sqrt{n^2+1}+1)/n\}}{\frac{2}{3}(n^2-1)(n^2+1)^{\frac{3}{2}}} \quad (38)$$

$$l_{m,\perp}^{(0)} = \frac{2}{5}(n^5-1)/(n^2-1) \quad (39)$$

where n is the relative refractive index ($n \equiv n_2/n_1$). In our experimental conditions, $n_1 = 1.5$ (polymer) and $n_2 = 1.0$ (air). Therefore, we obtained $[L(z_0)/L(\infty)]_\parallel = 0.92$ and $[L(z_0)/L(\infty)]_\perp = 0.33$. The fluorescent probe, PDI, has $k_{nr}(\infty)$ and $k_{nr}(\infty)$ of 5×10^6 s^{-1} and 2.5×10^8 s^{-1}, respectively. We calculated orientation (θ) dependent $\Phi_{nr}(z_0)$ using those values and equation 33. The results are displayed in Figure S5. As is obvious from the figure, the brightness (fluorescence quantum yield) of PDI located very close to the interface is virtually independent of the molecular orientation.

References

1. Lukosz, W. *Journal of the Optical Society of America* **1979,** 69, (11), 1495-1503.
2. Lukosz, W.; Kunz, R. E. *Journal of the Optical Society of America* **1977,** 67, (12), 1607-1615.
3. Lukosz, W.; Kunz, R. E. *Optics Communications* **1977,** 20, (2), 195-199.

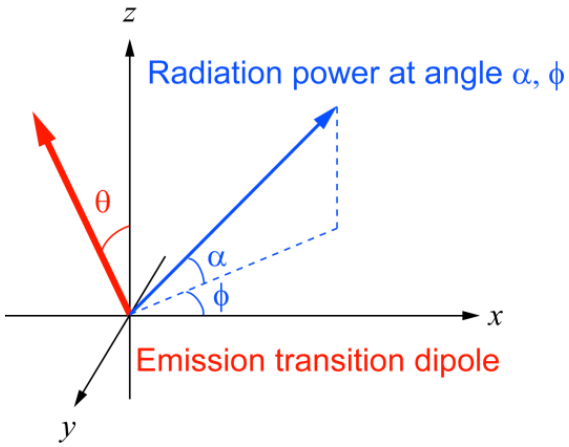

Figure S1. Schematic diagram of the orientation of emission transition dipole and radiation power at angle α, ϕ.

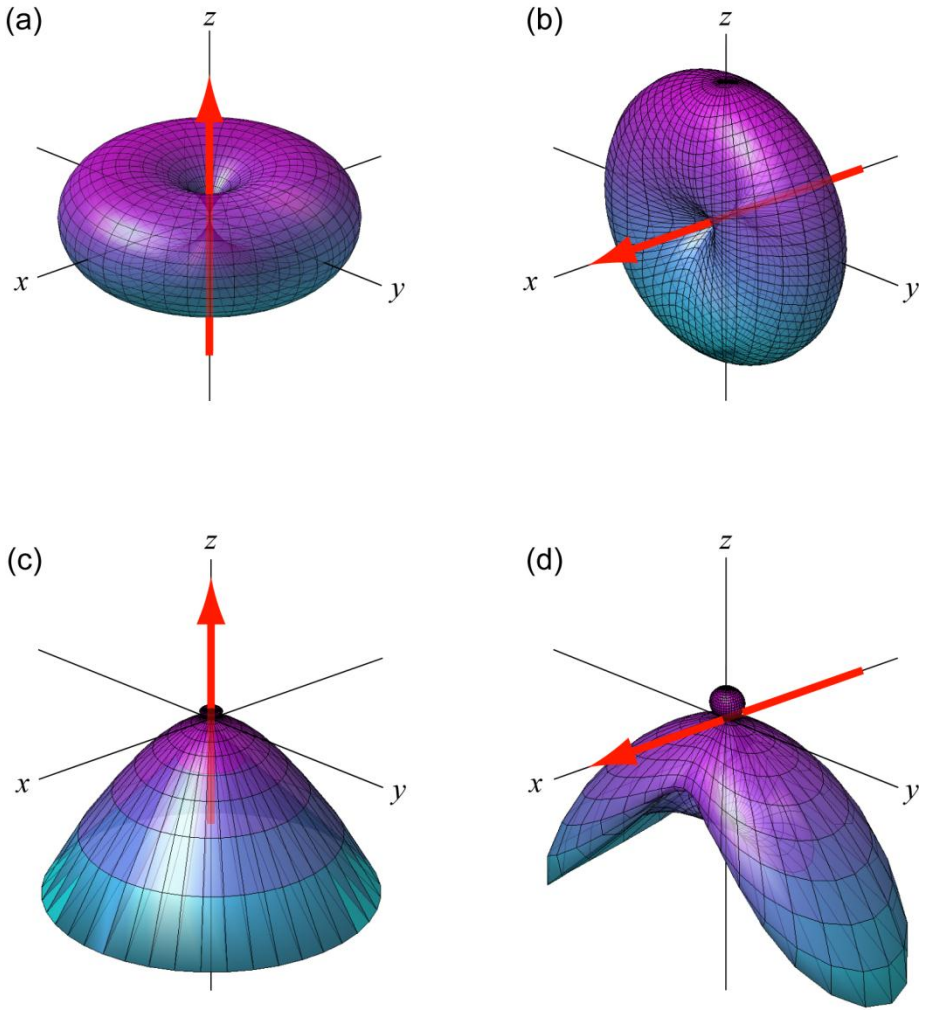

Figure S2. Radiation patterns of dipoles (a, b) in a homogeneous medium and (c, d) at a plane dielectric interface (x-y plane, n_1 = 1.5, n_2 = 1.0). The red arrows show transition dipole orientation.

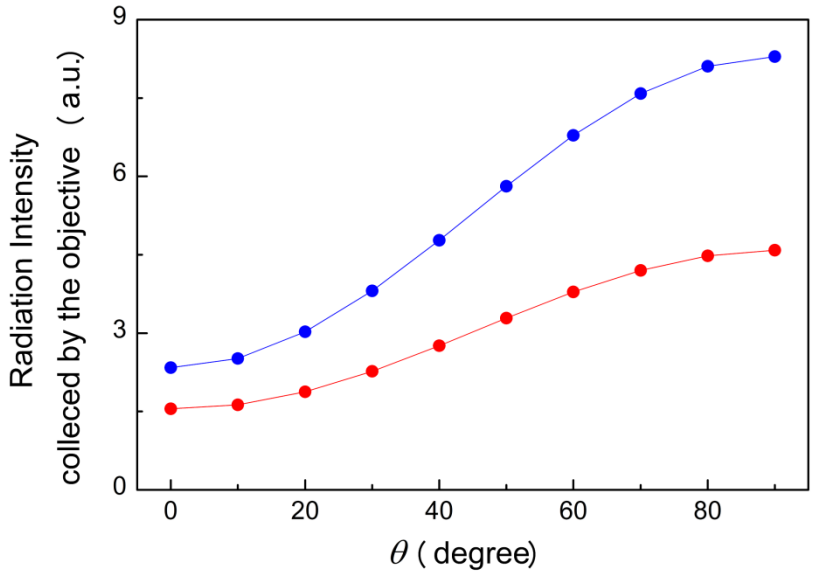

Figure S3. Orientation dependent fluorescence intensity collected by the microscope objective (N.A. 1.3). The red and blue data points were obtained for the molecule in a homogeneous medium and at a plane dielectric interface (n_1 = 1.5, n_2 = 1.0), respectively.

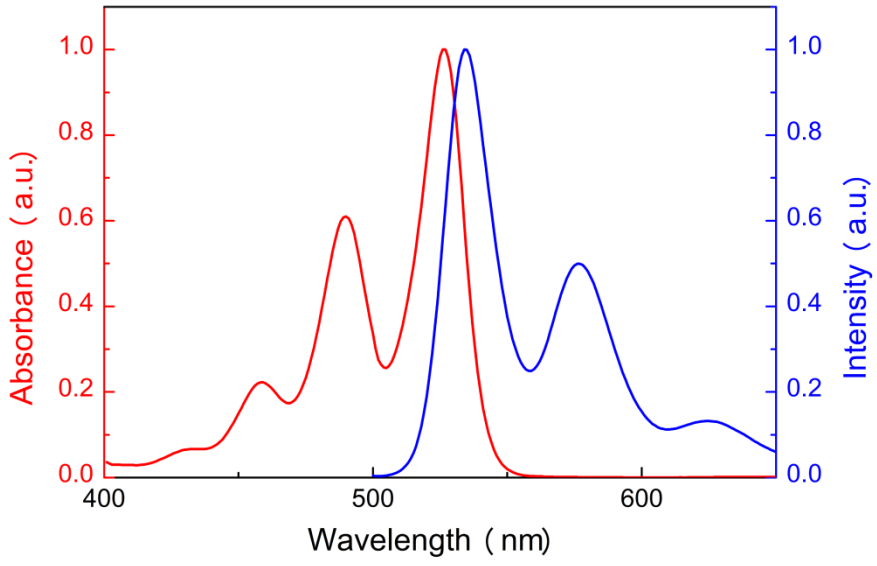

Figure S4. Bulk phase absorption and fluorescence spectra of PDI in toluene.

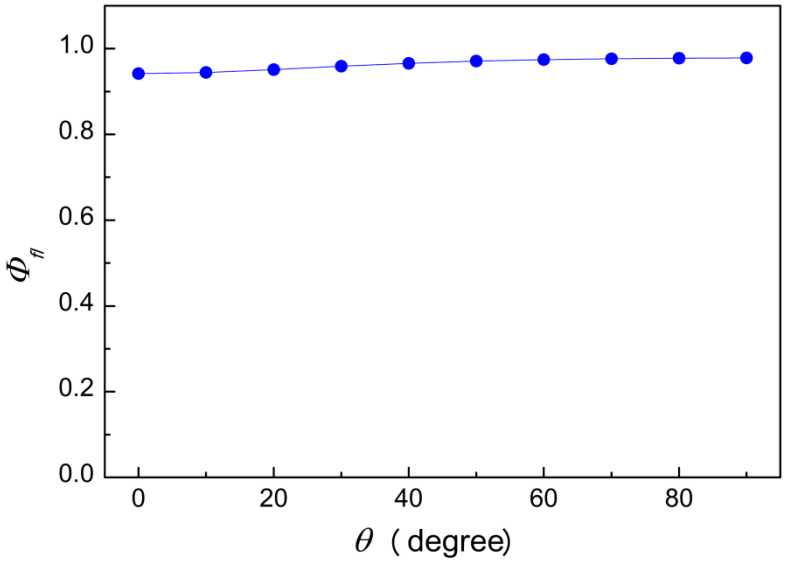

Figure S5. Orientation dependent fluorescence quantum yield of PDI located at a plane dielectric interface (n_1 = 1.5, n_2 = 1.0).

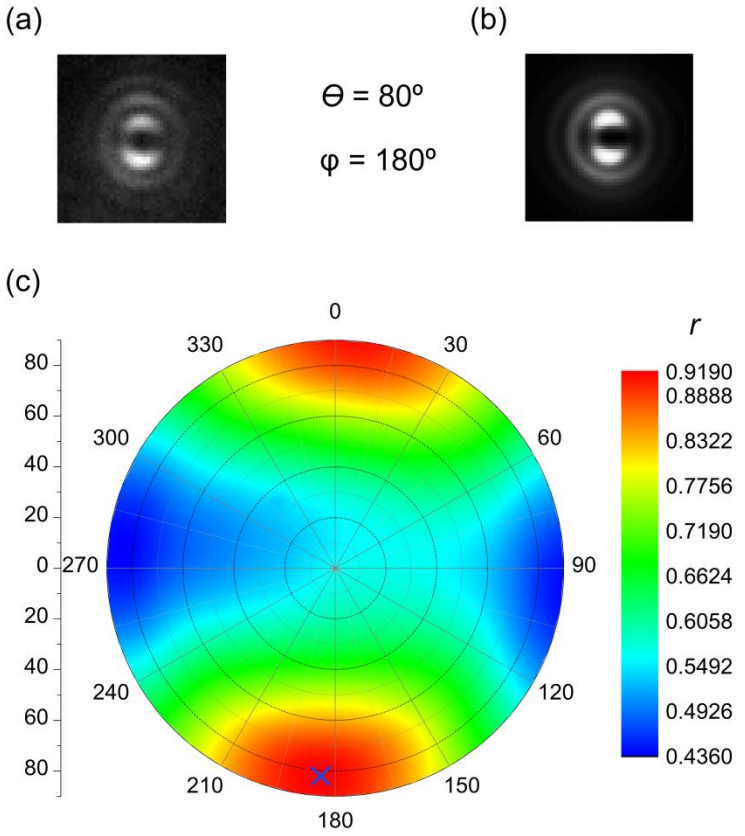

Figure S6. (a) Example of single-molecule defocused fluorescence image of PDI. (b) Theoretically calculated defocused image which provides largest value of correlation coefficient (θ = 80°, ϕ = 180°). (c) Polar plot of the correlation coefficients obtained from the 2 dimensional correlation analyses. The cross mark shows the angle (θ and ϕ) which provides a largest correlation coefficient.

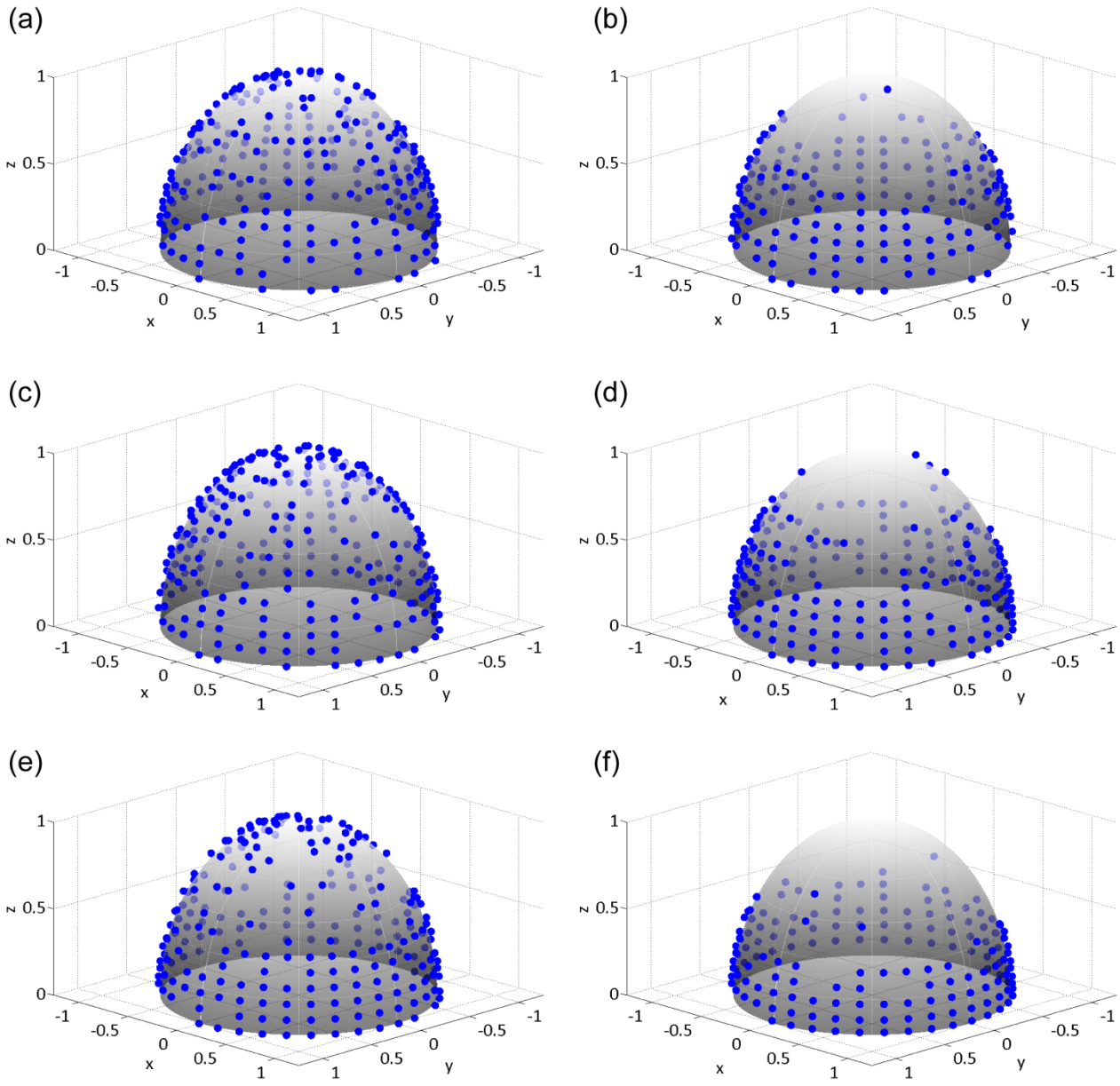

Figure S7. Experimentally obtained 3 dimensional orientation of PDI molecules embedded in (a, b) 60 nm thick PMA, (c, d) 300 nm thick PMMA, and (e, f) 100 nm thick PMMA films. The data were obtained by either (a, c, e) multi-beam- or (b, d, f) epi-illumination conditions.

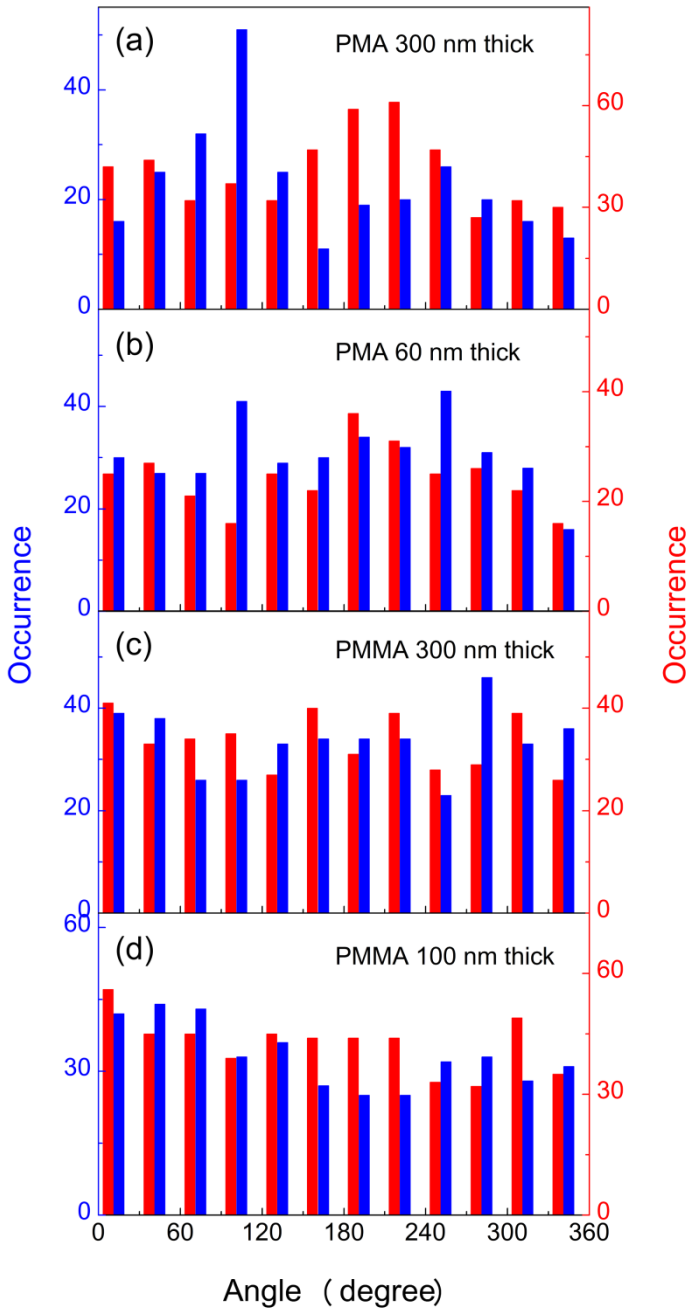

Figure S8. Frequency histograms of azimuth angle ϕ determined for individual PDI molecules embedded in (a) 300 nm thick PMA, (b) 60 nm thick PMA, (c) 300 nm thick PMMA, and (d) 100 nm thick PMMA films. The red and blue histograms were obtained through the experiments with the epi- and multi-beam-illumination.

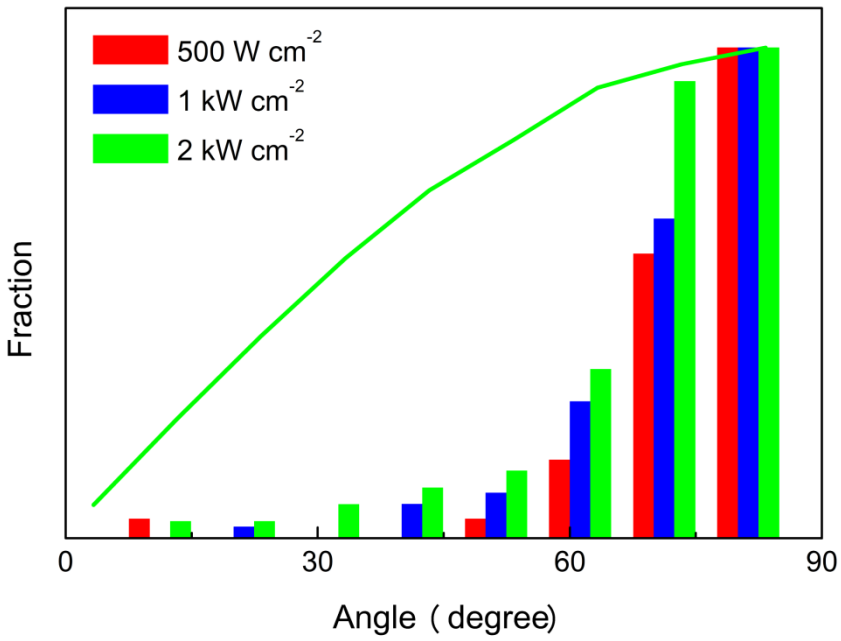

Figure S9. Frequency histograms of out-of-plane angle θ determined for individual PDI molecules embedded in a 300 nm thick PMA film with epi-illumination condition. The red, blue, and green histograms were obtained using the excitation power of 0.5, 1, and 2 kW cm^{-2}, respectively.The solid line represents orientation distribution expected for randomly oriented molecules in a thin film.